Facies (2025) 71:13
https://doi.org/10.1007/s10347-025-00705-5

ORIGINAL ARTICLE

An Ediacaran trace-like body fossil of a *Palaeopascichnus* specimen from Oman under 3D micro-tomography

André Jorge Pinto[1] · Pedro Álvarez-Lloret[2] · Ivan Callegari[3] · Andreas Scharf[4]

Received: 21 March 2025 / Accepted: 16 June 2025

Abstract

Palaeopascichnus is an Ediacaran organism, whose phylogenetic affiliation and functional anatomy are both shrouded in mystery. Different studies and assessments have interpreted this fossil as macrophytes or foraminifera-like protists. Currently ongoing discussions concerns the possible phylogenetic relation between *Palaeopascichnus* and modern xenophyophores; benthic organisms that built agglutinated tests. We present micro-XRD, SEM-EDS and three-dimensional microtomographic data on a possible *Palaeopascichnus* specimen from the Ediacaran Fara Formation, in Wadi Bani Awf, Jabal Akhdar, Oman. The unique preservation of this specimen as a full positive epirelief of drusy calcite growths represents a new taphotype for this organism, enabling a more accurate observation of chamber structure and better morphological characterization. The data gathered concerning both chamber´s dimensions and morphology does not point towards an affiliation with any known *Palaeopascichnus* species, except for much smaller *P. jiumenensis*. Therefore, it is possible that this specimen represents a new, previously unknown species.

Keywords *Palaeopascichnids* · X-ray micro-tomography · Fara formation · Wadi bani awf

Introduction

The Ediacaran fossil *Palaeopascichnus* has been the object of continuous controversy to the present day in the literature. In fact, its very nature as either a trace or body-part fossil was initially contentious, and the organism´s phylogenetic affinities remain currently unclear. Despite several studies describing *Palaeopascichnus* as an ichnofossil (e.g. Glaessner 1985; Palij 1976; Fendonkin 1981), such early/primary interpretation has been repeatedly dismissed and replaced by assessments pointing towards affinities with macrophytes (Haines 2000), or foraminifera-like protists (Seilacher et al. 2003, 2005; Seilacher and Mrinek 2011; Kolesnikov et al. 2018). An ongoing debate focuses on a possible phylogenetic affiliation between *Palaeopascichnus* and modern xenophyophores, benthic organisms, which built agglutinated tests. While Antcliffe et al. (2011) gathered a compelling set of stratigraphic and structural arguments contrary to such attribution, Kolesnikov et al. (2018) discovered striking structural similarities between *Palaeopascichnus lineraris* and *Aschemonella monela*. Gehling and Droser (2009) envisaged *Paleopascichnus* as a type of epi-benthic organism, whose size and shape pose problems to taxonomic assessments. Taphonomic considerations by

✉ André Jorge Pinto
andrejor@ucm.es

Pedro Álvarez-Lloret
pedroalvarez@uniovi.es

Ivan Callegari
ivan.callegari@gutech.edu.om

Andreas Scharf
scharfa@squ.edu.om

[1] Department of Mineralogy and Petrology, Faculty of Geological Sciences, University Complutense of Madrid, C/ José Antonio Novais, 12, Madrid 28040, Spain

[2] Department of Geology, Faculty of Sciences, University of Oviedo, C/ Jesús Arias de Velasco, s/n, Oviedo 33005, Spain

[3] Applied Geoscience Department, German University of Technology in Oman, P.O. Box 1816, Athaiba PC 130, Sultanate of Oman

[4] Department of Earth Sciences, Sultan Qaboos University, 123, Al-Khod, Athaiba, Sultanate of Oman

Published online: 23 June 2025

the latter authors suggest the possibility of bacterial mats serving as ecological substrates for palaeopascichnids. Furthermore, Kolesnikov et al. (2018) identified the lack of diversified taphonomic perspectives in previous investigations and the possible impact of taphonomy on the morphology of preserved fossils, as shortcomings entangling the phylogenetic determination for these organisms. Considering the challenges, Kolesnikov and Desiatkin (2022) recognized six valid species of Palaeopascichnid, based on the morphological observations of > 1,200 specimens from different geographical locations and sedimentary contexts. In this respect, the latter authors also gathered significant statistical data reflecting palaeoecological variations among the different identified species.

Palaeopascichnus fossils have been found in several locations, dispersed across northeastern North America, Europe, and Asia. Reported occurrences with variable specimen abundance related to settings in the East European Platform (e.g. Podolia, Central and South Urals, Moscow and Mezen basins, Timan Range), Arctic Norway (Digermulen Peninsula), North and South China, Avalonian lithologies both in Newfoundland and Wales, Australia (Adelaide Rift Complex), and Siberia (Olebek Uplift) (Cope 1982; Dong et al. 2008; Fedonkin 1981; Gehling and Droser 2009; Haines 2000; Jensen et al. 2018; Kolesnikov et al. 2018, 2023; McIlroy and Brasier 2017; Palij 1976; Yuan et al. 2011).

In the present study, we focus on the morphological and taphonomic characterization of a possible *Palaeopascichnus* specimen discovered in Wadi Bani Awf, Oman, based on observations related to the three-dimensional structure of the fossil, and both chemical and mineralogical compositions of the different structures that constitute it. Different analytical characterisation techniques have been used: three-dimensional micro-computed tomography (μCT), X-ray diffraction (XRD) and energy dispersive X-ray spectroscopy (EDS) studies. The Ediacaran Fara Formation outcrops in Wadi Bani Awf, so the discovery of this specimen in its Upper Member represents a contribution to the geochronological and geodynamic characterization of Eastern Arabia, especially concerning geological events described by Callegari et al. 2020), (2025); Scharf et al. (2021a). The data gathered in the present research shed light on the specific taphonomic conditions that enabled the exceptional level of preservation of this *Palaeopascichnus* fossil specimen, and possible classification pathways.

Geological background and specimen provenance

The Oman Mountains of the eastern Arabian Peninsula comprehend a wide range of geological formations ranging from the Tonian to the Neogene and are characterized by mostly by siliciclastics and carbonates (e.g., Glennie et al. 1974; Scharf et al. 2021b; Fig. 1). The latter rock successions are divided in two parts by an angular unconformity, between Autochthonous units A and B. These two tectonostratigraphic units are characterized in the Jabal Akhdar Dome by Cryogenian to Ediacaran (Autochthonous A), and Permo-Mesozoic (Autochthonous B) formations (Fig. 1b).

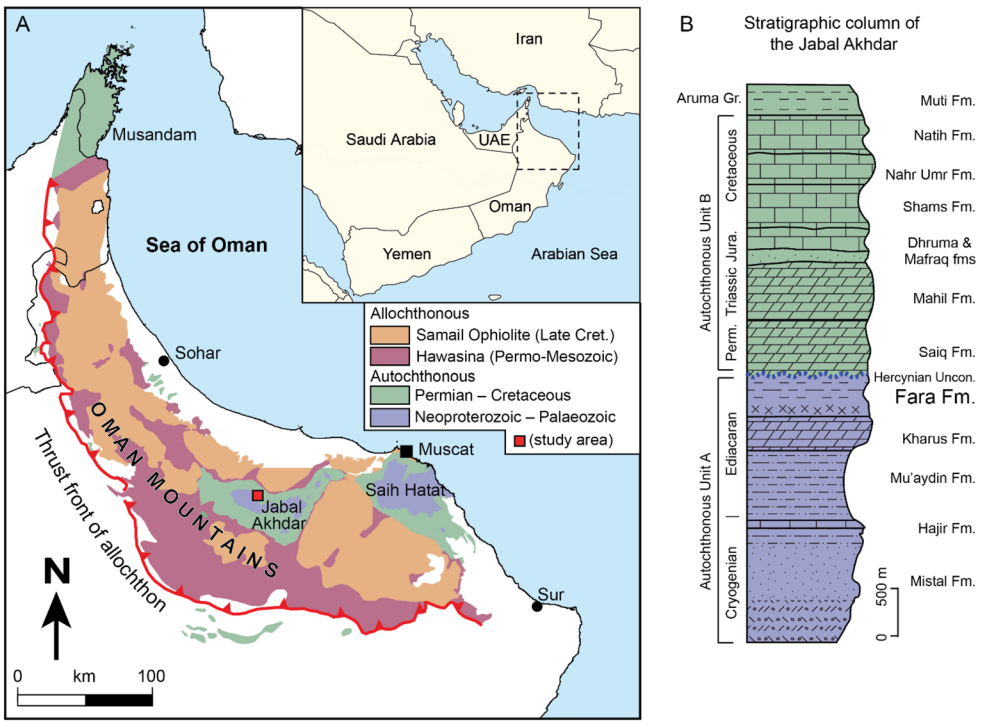

Fig. 1 Geological map of the Oman Mountains after Forbes et al. (2010) and Callegari et al. (2025)

The core of the Jabal Akhdar Dome comprises the following formations (Béchennec et al. 1993): the Cryogenian Mistal Formation, is a siliciclastic sequence consisting of an alternation of siltstones, sandstones, and diamictites (e.g., Beurrier et al. 1986), with tuffaceous beds of U-Pb zircon age of ~720 Ma (Brasier et al. 2000; Bowring et al. 2007) in its upper section. The next younger formation, the Ediacaran Hajir (or Khufai, subsurface equivalent) Formation, consists of dark carbonates with stromatolites. The siliciclastic Ediacaran Mu'aydin (or Shuram, subsurface equivalent) Formation follows the Hajir Formation, with a thickness of 800 m (Beurrier et al. 1986; Mattern and Scharf 2019), and the Ediacaran Kharus (or Buah, subsurface equivalent) Formation overlies the Mu'aydin Formation, with a thickness of <245 m. The Ediacaran Fara Formation is the youngest Neoproterozoic formation within the Jabal Akhdar Dome, with a thickness of <412 m, and displays various lithologies, including carbonates, cherts, volcaniclastics, siltstones, sandstones, and conglomerates (Beurrier et al. 1986; Callegari et al. 2025). The Neoproterozoic formations are overlain by the Upper Permian Saiq Formation, belonging to Autochthonous B, at an angular unconformity.

The age of the Fara Formation is presumed to be Neoproterozoic to earliest Cambrian (Beurrier et al. 1986; Bowring et al. 2007; Forbes et al. 2010 and references therein). However, Callegari et al. (2025) assigned an entirely Ediacaran age for this formation, based on geochemical information. Furthermore, they found an Ediacaran fossil (possible *Palaeopascichnus linearis*) within the upper section of the Fara Formation. This fossil is the object of the present work.

The lithology of the Fara Formation differs from the supposed time-equivalent subsurface rocks of interior and southern Oman. In fact, the Ara Group in the subsurface of the interior of Oman is characterized by a carbonate-evaporite sequence with thick salt deposits, which accumulated in a transpressional/transtensional basin setting (e.g. Mattes and Conway Morris 1990). However, some shale and silica-rich sedimentary deposits occur in the subsurface of southern Oman. The thick Ara evaporitic successions were deposited in geographically restricted and NNE/SSW-striking basins during periods of low relative sea level, where stratified, anoxic conditions periodically prevailed, and organic-rich sediments and salt were deposited (Amthor et al. 2003). The rocks of the subsurface Ara Group records segmentation of the regionally extensive Nafun Basin into three smaller basins represented by the subsurface salt basins in Oman. The carbonate–evaporite succession of the Ara Group in the southern Oman is the potential time-equivalent to the peritidal carbonate succession in the Huqf area.

The Wadi Bani Awf area of the Jabal Akhdar Dome contains the Kharus and Fara formations, which are important for understanding the geological history of the region. The Kharus Formation was deposited in a tidal flat environment and is characterized by stromatolite-bearing carbonates (e.g. Cozzi et al. 2004). Carbonate samples from the lowermost and uppermost parts of the Kharus Formation have been dated using the U-Pb in calcite technique, with obtained ages of 573±28 and 564±4.5 Ma, respectively (El-Ghali et al. 2021).

The Fara Formation has been divided into three members, comprising different lithotypes, including cherts, dolostones, conglomerates, siltstones, breccias, and sandstones (e.g. Beurrier et al. 1986; Callegari et al. 2025). An ignimbrite level within the Fara Formation has been dated at 544.5±3.3 Ma using U-Pb on zircons (Brasier et al. 2000). Further U-Pb zircon ages from volcanics in the Fara Formation suggest a weighted mean age of 547.23±0.28 Ma for the base and 542.54±0.45 Ma for the top of the formation (Bowring et al. 2007). This ignimbrite lithologies are stratigraphical suprajacent to the fossil-bearing level within Fara Formation, and its detailed petrographic description can be found in Pinto et al. (2020) and the extensive revision of Callegari et al. (2025). Figure 2 displays a simplified geological map of the area described here, depicting the location (P) where the specimen under analysis was collected.

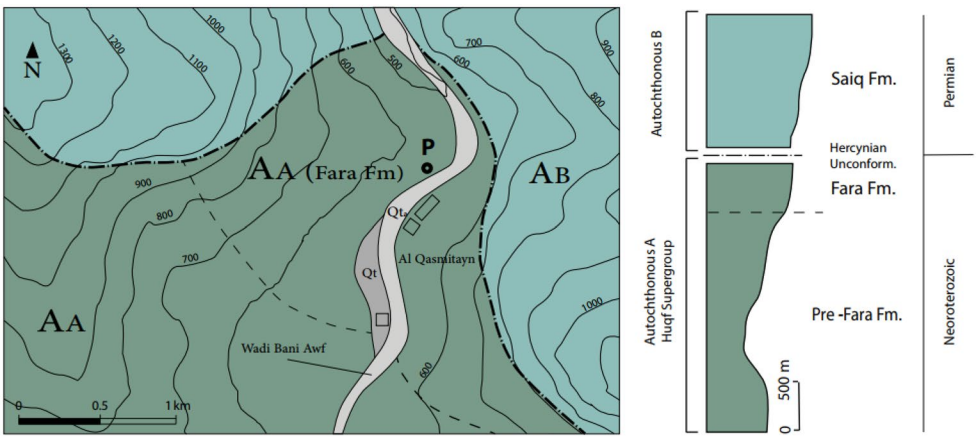

Fig. 2 Simplified geological map and fossil collection site (P, 23° 17' 13.48" N 057° 27' 58.11" E, 550 m alt.), including the Hercynian Unconformity (dash and dot black line) at Wadi Bani Awf. AA: Autochthonous A, AB: Autochthonous B, Qt: Quaternary terraced alluvial deposits, Qt_a: Quaternary alluvial deposits. The dashed black line marks the boundary between Ediacaran Fara Formation and Ediacaran pre-Fara formations, modified after Pinto et al. (2020)

Specimen occurrence and identification

The specimen occurs on the top bedding plane surface of a quartz siltstone rock, located about 65 m below the top of the Fara Formation (Figs. 2 and 3, inset), embedded in a superficial coating of carbonate. The overlying bedding surface was shattered during sample collection, and therefore no existing negative relief has been lost. Given its uniqueness, the question arises on the possible biologic (i.e. fossilized body parts, ichnofossil), sedimentary, or diagenetic/post-diagenetic inorganic origins of this specimen. Sedimentary structures with similar morphologies have never been reported in scientific literature concerning Fara Formation, or elsewhere. The same applies to abiogenic diagenetic, or post-diagenetic mineral processes that could produce the observed external shape of this specimen. Therefore, we have considered the object as a series of fossilized body parts of an Ediacaran organism, most specifically *Palaeopascichnus*, as recently identified by Callegari et al. (2025).

Figure 3 displays the fossil-bearing sample, where the specimen appears as a uniserial arrangement of discoid, saucer-shaped ridges, with a total length of ~ 7.5 cm. A possible alternative of identification could be an Ediacaran xenophyophore, especially *Neonereites*. However, the comparison of published morphological imaging of the latter (e.g. Palij et al. 1979; Seilacher 2007; Acenolaza et al. 2009) with the specimen under study reveals insurmountable differences. While the fossilized structures shown in Fig. 3 are clearly discoidal and saucer-shaped, *Neonereites'* chamber-like elements are globular. Furthermore, in line with the general remarks of Gehling and Droser (2009) about palaeopascichnids, this specimen lacks any textural evidence indicating the occurrence of agglutinated tests, typical of xenophyophores. The discussion of a possible phylogenetic association between xenophyophores and palaeopascichnids is nonetheless beyond the scope of the present investigation, which focuses on morphological characterization of a single specimen.

Despite the intensive survey efforts taken during several field trips to Wadi Bani Awf, the research team was unable to find any other specimens in the Fara Formation. The following section discusses the possible influence of taphonomy on scarcity.

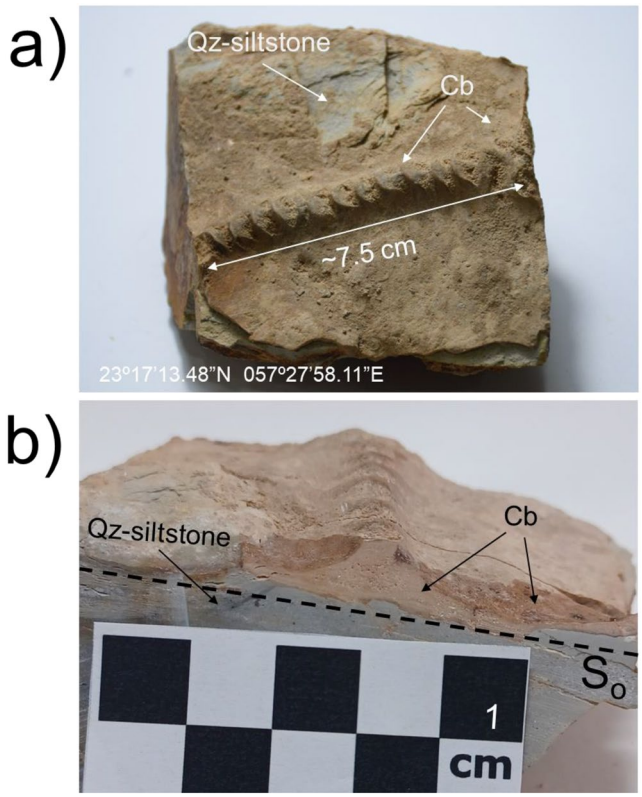

Fig. 3 Fossil specimen collected from the exposed segment of Fara Formation in Wadi Bani Awf, Oman, in **a**) plane view, and **b**) cross section view, transversal to the uniserial arrangement of discoidal ridges. See text for the detailed geological background. Geographical coordinates correspond to WGS84 system (World Geodetic System). Qz = quartz, Cb = carbonate, S_0 = bedding plane

Materials and methods

A small slab of the specimen was cut perpendicularly to the bedding plane, embedded in resin, and processed into a thin section for observation under a polarizing petrographic microscope.

The whole fossil specimen was analyzed using X-ray computed axial microtomography using a Xradia 510 Versa (ZEISS) at the Centro de Instrumentación Científica (University of Granada, Spain). This X-ray imaging equipment allows the visualization of the distribution patterns of materials with different attenuation values through a reconstruction of sets of parallel cross-sections, perpendicular to the axis of rotation within the scanner. The following consistent experimental settings were established: 0.4 × magnification, 24.705 µm voxel size, 208 mm source-sample distance, 80 mm detector–sample distance, and 4001 projections. Voltage, current, filter and exposure time were adjusted to 140 kV accelerating voltage, 71 µA beam current, 45 s exposure time and HE2 source filter. Image reconstruction was done with Reconstructor Scout and Scan™ (ZEISS) using a 0.5 Recon filter, corrected by a center shift of 2.525 pixels and 0.120 beam hardening. Dragonfly Pro™ (Object Research System) was used for advanced post-processing analysis and three-dimensional image measurements.

The identification of the mineral phases of the different structures of the fossil specimen was carried out by X-ray diffraction (XRD) technique. Two-dimensional XRD (2D-XRD) patterns were obtained using a Bruker

D8 DISCOVER diffractometer equipped with a 2D detector (DECTRIS PILATUS 3 100 K-A) using CuKα radiation (λ = 1.5406 Å) at 50 kV and 30 mA. The 2θ scanning angle ranged from 5° to 80°, considering 2θ steps and 30 s/step focused with a pinhole collimator of 1 mm in diameter. The analyzed spots in a transversal section of the specimen were selected by employing an optical microscope equipped with a laser reference (one 2D-XRD frame per 1 mm across the section). The diffraction intensities concentrated in arcs (corresponding to specific d-spacing) were integrated into a unidimensional scan (i.e. 2θ pattern). Diffraction pattern interpretation was performed using X´Pert Plus software coupled with PDF-2 X-ray database.

Electron microscope imaging was carried out using an environmental scanning electron microscope (ESEM, FEI, mod. Quanta 400) operated at 20 kV voltage and 10 mA current. Energy dispersive x-ray spectroscopy (EDS, BRUKER xFlash 6/30 detector) was employed to estimate the element relative concentrations on a transversal surface of the fossil specimen.

Results

Sample petrography

Figure 4 depicts transmitted plane-polarized light micrographs of a transverse section (perpendicular to the bedding plane) of a skeletal unit of the specimen and the underlying lithological substrate, parallel to the surface exposed in Fig. 3b. As shown in Fig. 4a, the fossilized structure corresponds to drusy growths of carbonate columnar grains with their main symmetry axis radiating perpendicularly to the bedding plane (S_0). Such orientation of carbonate individuals necessarily implies crystal growth in an open space, in this case enclosed by the organism´s skeletal structures, here named “chambers” for convenience. The fibrous growth occurs in consecutive parallel layers defined by thin dark (isotropic) bands, in which crystal sizes appear homogeneously in the central zone of the chamber volume. However, distinct variations in crystal size can be observed between the different layers, since those closer to the bedding plane are finer grained, becoming progressively coarser towards the core of the chamber.

Strikingly, the drusy growths in chambers grade laterally into the fine-grained calcite precipitate on the bedding plane, as shown in Fig. 4b. Both lateral and vertical crystal size gradations pose limitations to the exact placement of chamber boundaries using merely optical criteria. The carbonate mineralization occurs on the top bedding surface of a very fine-grained quartz siltstone belonging to the Fara Formation, characterized by sub-millimetric, sub-angular to sub-rounded quartz grains embedded in a clay matrix. The detrital fraction is cemented by carbonate precipitate. A more detailed mineralogical analysis of the underlying sandstone will be tackled by means of both micro-XRD and ESEM-EDS analyses.

In view of the aforementioned mineralogical features, it can be concluded that this fossil specimen consists of a well-developed and preserved positive epirelief, comprising an internal secondary filling of chambers, derived from several dissolution-growth cycles of carbonate. Aqueous fluids of superficial origin may have easily mobilized carbonate and other ions from the surrounding lithologies, thus supplying the necessary chemical components to the mineralized zones.

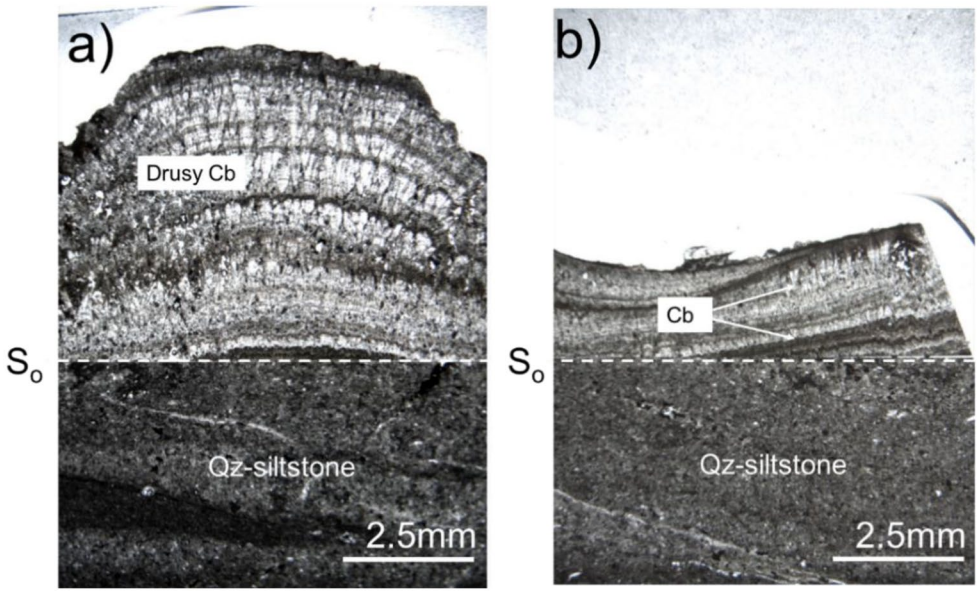

Fig. 4 Transmitted plane-polarized light micrographs of a transversal section of the fossil specimen, focusing on **a**) the central portion of a chamber, and **b**) lateral termination. Qz = quartz, Cb = carbonate, S_0 = bedding plane

Mineralogic phase identification and chemical analysis

Transverse section reconstruction of the specimen by ESEM micrographs shows different structures associated with the substrate and the fossil chamber (Fig. 5a). The substrate, corresponding to the bedding plane in which the fossil lies, presents a consolidated solid structure with some large mineral grains.

Throughout the fossil body unit, a progressive decrease in porosity (vertical gradation) is observed from the substrate limit to the boundary of the chamber. Thus, the intervening space between the substrate and the edge of the fossil chamber appears to be filled by a secondary mineral deposition, as also described by transmitted plane-polarized light observations.

The detailed ESEM micrographs of the fossil and substrate areas (Fig. 5b1 and c1, respectively) show different distribution of elements. EDS analysis representations of the fossil area display the relative abundance of mainly calcium and lesser silicon content at the chamber boundary (Fig. 5b2-b5).

This elemental distribution agrees with the identification of mineral phases present in the fossil chamber, determined by XRD analysis (see below). Nonetheless, EDS analyses of the substrate (Fig. 5c2-c5) show a greater variety of heterogeneously distributed elements. The distribution for silicon and aluminum (Fig. 5c3-c4) displays higher concentrations in sub-rounded and sub-angular grain boundaries (the latter with larger dimensions), while calcium (Fig. 5c5) seems to fill the intergranular space. These major elements and the balance in lower relative abundance (e.g., Cl, K, Fe, Mg; Fig. 5c5) are clearly associated with the mineral phases identified by subsequent XRD analyses.

Figure 6 shows the XRD analyses performed for the fossil and substrate areas, corresponding to the section previously observed by ESEM (image from Fig. 5a).

By means of a laser reference for focusing on the X-ray beam, the diffractometer allows the areas of interest to be located on the surface of the specimen. The two-dimensional detector acquires the different Debye-Scherrer rings (intensity arcs) corresponding to the diffraction planes of the mineral phases present at each analyzed position.

The fossil chamber boundary (Fig. 6a1) yielded a two-dimensional pattern (2d-XRD) with intensities homogeneously distributed along the diffraction arcs (Fig. 6a2). The integration of the 2d-XRD pattern provides a one-dimensional scan (Fig. 6a3; 2-theta) in which a phase predominantly of calcite and in a lesser proportion of quartz is identified for the boundary of the fossil chamber. The XRD analysis along the specimen surface (i.e. intervening space between the edge of the fossil chamber and the limit of the substrate) resulted in the identification of these same mineral phases without any change in the crystalline properties (data not shown). The analysis of the substrate area (Fig. 5b1) yielded a 2d-XRD pattern (Fig. 6b2) in which crystalline spacings with different intensities are observed, corresponding to a polymineral association. The identification of the mineral phases from the 2-theta scan (Fig. 6b3)

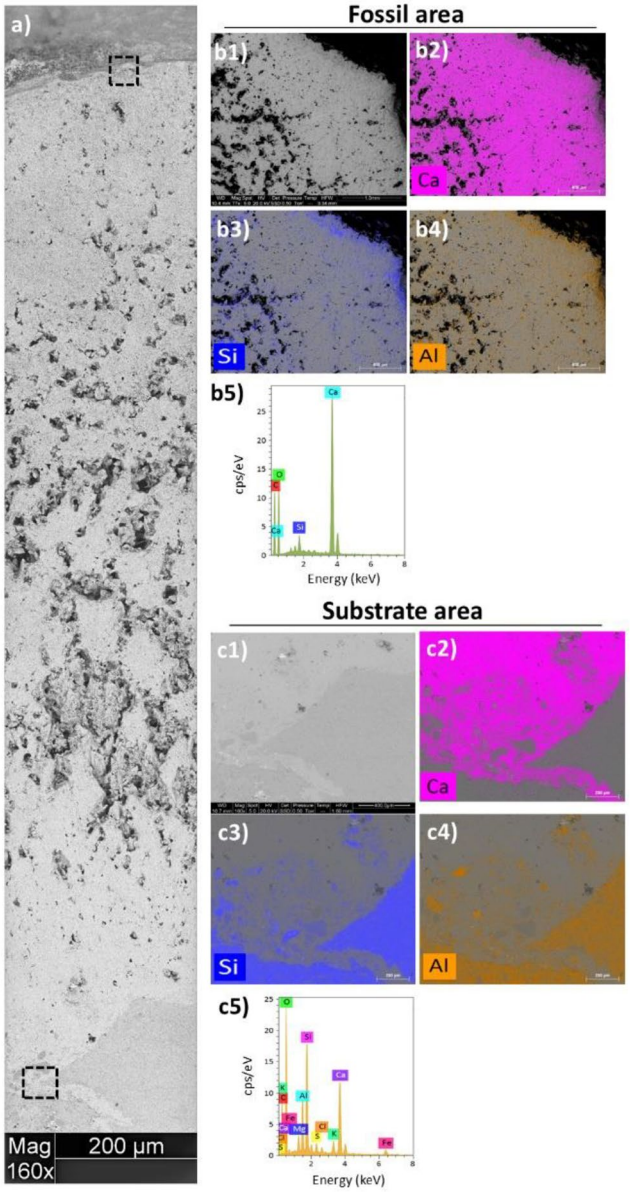

Fig. 5 ESEM micrographs and EDS analysis of the specimen. ESEM reconstruction of a transverse section of the specimen (**a**), showing the substrate (bottom) and a chamber unit of the fossil skeletal structure (top). Detailed ESEM micrographs of the areas (b1; fossil and c1; substrate areas) considered for EDS analyses. Representations for EDS analysis show relative elemental distribution and abundance of calcium (b2-c2; purple), silicon (b3-c3; blue), and aluminum (b4-c4; orange). Average total elements abundance for the EDS areas analyses (b5-c5)

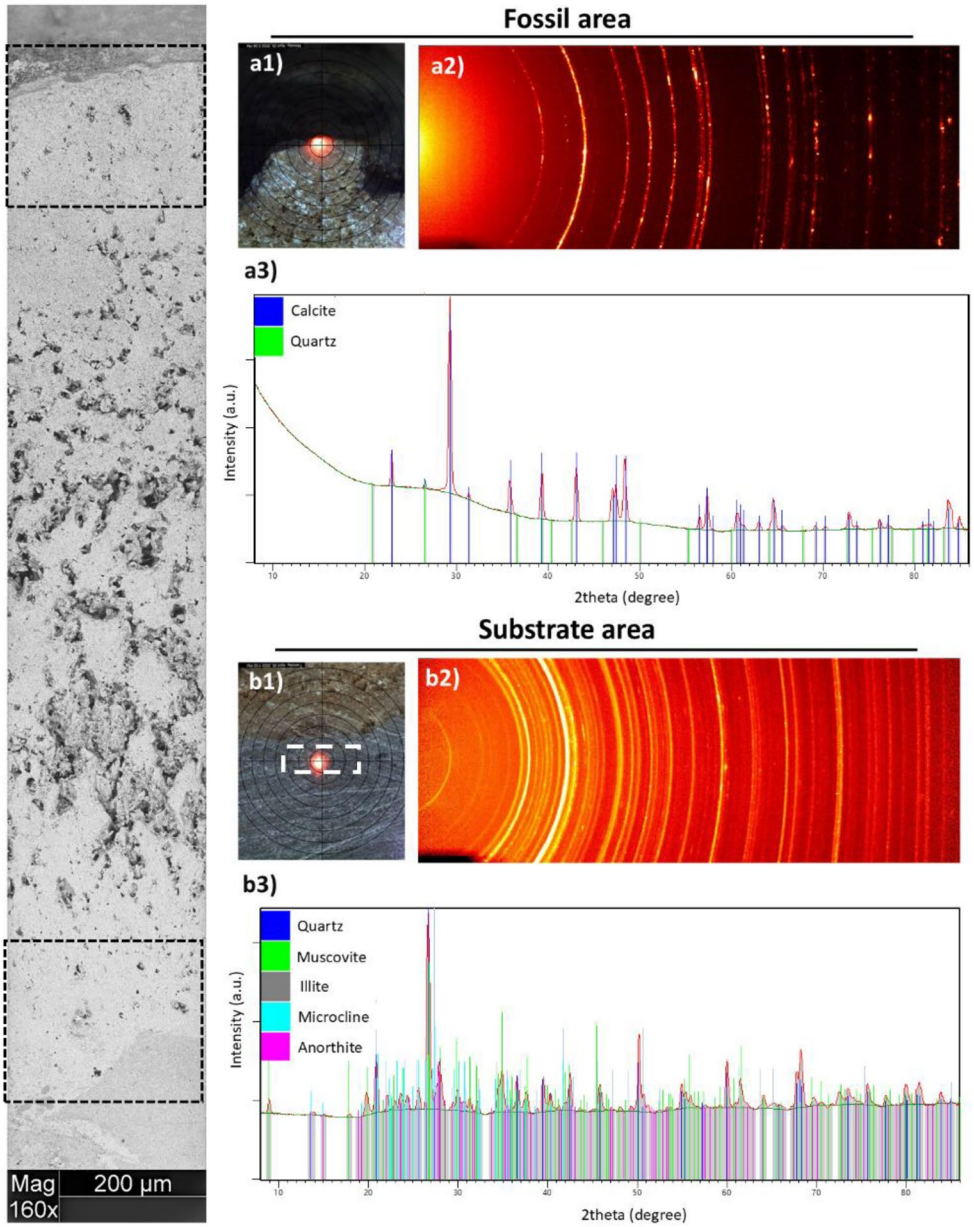

Fig. 6 ESEM image reference and X-ray diffraction (XRD) analysis of the specimen corresponding to the fossil (**a**) and substrate (**b**) areas. a1) Location of the analysis point by laser reference at the fossil´s chamber edge. a2) 2d-XRD pattern showing the Debye-Scherrer rings (diffraction arcs) of the mineral phases present in the fossil. a3) One-dimensional scan (2-theta pattern) from the integration of the 2d-XRD pattern, indicating the assignment of calcite and quartz as mineral phases present in the fossil. b1) Location of the analysis area of the substrate. b2) 2d-XRD pattern corresponding to the substrate. b3) Assignment of mineral phases present in the substrate: quartz, muscovite, illite, anorthite and microcline

indicates the presence of calcite, quartz, muscovite, illite, anorthite, and microcline in the substrate area.

Morphological features by microtomographic analysis (µCT): 3D morphological features

Figure 7a displays a micro-tomographic reconstruction of the entire fossil specimen, obtained along an orientation that allows the visualization of the linear sequence of protruding ridges, identified as the chambered skeleton of *Palaeopascichnus*. The homogenous contrast in Fig. 7a confirms that these composing materials have similar density, in view of the depicted small variations of X-ray attenuation.

The shape of the chambers observed on this surface can be described as discoidal ridges. The arrangement of the various skeletal components is not perfectly aligned, following a slightly curved trajectory. Furthermore, the chambers are not seated in a completely flat lying plane, the frontal chambers being nearer the viewer in Fig. 7a laying in slightly lower plane with respect to the anterior chambers, situated in the farthest extremity from the viewer. At the latter extremity, it is possible to observe a bifurcation of chambers, outlined by a dashed box in Fig. 7a, preceded by a wider chamber with two joined ridges.

Figure 7b shows a shallow micro-tomographic slice taken along a plane parallel to the bedding plane, depicting the location of chamber bifurcation at an angle of ~38°. The

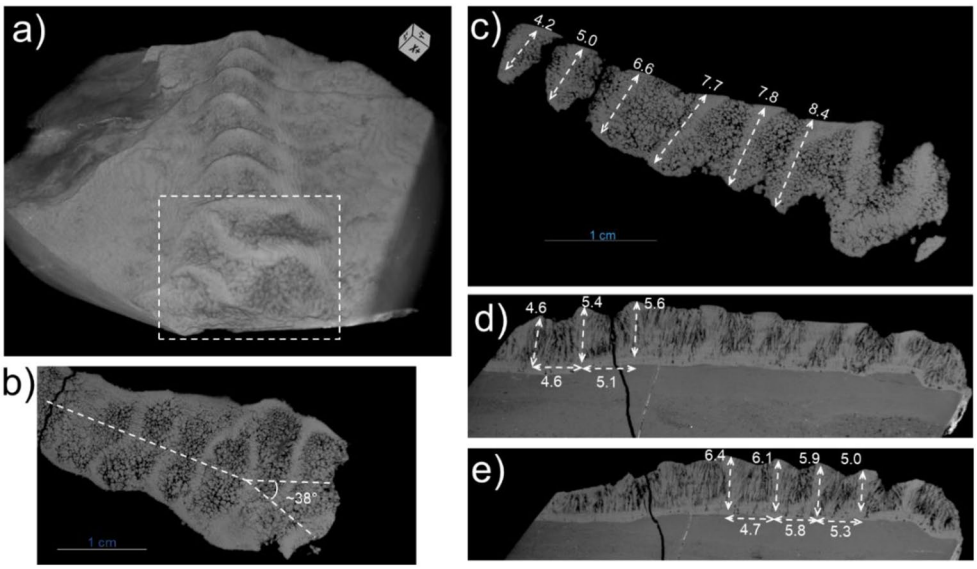

Fig. 7 Microtomographic reconstruction of the *Palaeopascichnus* specimen taken along different planar slices (see text for a further detailed explanation). The dashed box in a) delimits the zone of chamber bifurcation. All measurements are expressed in millimeters

narrow stripes of lighter color correspond to the central portion of chambers, characterized by a higher level of X-ray attenuation levels (i.e. relatively denser materials). However, considering the obtained XRD results and SEM observations, such does not reflect a chemical heterogeneity, but rather variations in calcite crystal size, which is larger in the core of the chambers, with a resultant lower porosity than volumes where smaller calcite precipitation occurs. These volumes with higher density may not correspond to the total chamber volume. Figure 7b reveals that the discoidal shape of the chambers is curved, with the convex part of each chamber aligning with the concave of the following one. Figure 7c corresponds to a further inwards micro-tomographic slice (towards the bedding plane), parallel to that represented in Fig. 7b, but closer to the base of chambers, which partially lose their arcuate shape. Width (w) measurements taken in this slice along the zones of maximum density, yield values in the $4.2 < w(\text{mm}) < 8.4$, and chambers become increasingly thicker towards the direction of bifurcation. The chambers display a strikingly nearly constant length (l) of $1.5 < l(\text{mm}) < 2.0$.

Since the specimen is formed by chambers aligned in a curved pathway, measurements taken in longitudinal sections (i.e. perpendicular to the bedding plane) were performed in two separate micro-tomographic plane slices, corresponding to Fig. 7d and e. These data were acquired along longitudinal planes across maximum chamber height/thickness, the measurement of which corresponded to the areas of highest density, from the base to the top of the calcite drusy growths. Thickness (t) of the chambers varies in the range $4.6 < t(\text{mm}) < 6.4$ and increases until right before the bifurcation of the chambers. Along these sections, the denser calcite fillings display curved/tilted growth patterns, convex towards the direction of the bifurcated edge. An accurate measure of the chamber separation is impossible to discern in the present taphotype, although the continuous and merged character of the structures suggests a very short separation distance. Using the distance (d) measured between consecutive crests ($4.6 < d(\text{mm}) < 5.8$) it can be further deduced a near-constant inter-chamber separation.

Discussion

The mineralogical and morphological characteristics of the specimen here discussed embody a new taphotype for *Palaeopascichnus*, in addition to those described by Hawco et al. (2019). Though the latter authors report full positive epireliefs of palaeopascichnids from the Fermeuse Formation of Newfoundland (Canada), these show flattened morphologies and do not correspond to mineralized structures on a bedding plane. The same type of structural collapse and morphological flattening seems to affect the carbonate-preserved *Palaeopascichnus linearis* specimens from the Khatyspyt Formation, Arctic Siberia (Russia), studied by Kolesnikov et al. (2018). These specimens correspond to "true" fossils, since the latter authors gathered cathodoluminescence data indicating the existence of minimally re-crystallized skeletal parts, which are interpreted as agglutinated tests. While the type of conservation of the specimen from Oman is commonly typical of small-chambered *Palaeopascichnus* (Hawco et al. 2019), the unusual taphonomic conditions reflected by the specimen from Wadi Bani Awf allowed the preservation of full positive epirelief of large chambers. Although the drusy calcite of the described specimen cannot be ascribed to a specific sedimentary genetic process, the absence of pressure-solution textural features suggests post-diagenetic crystallization as a likely mechanism. Such

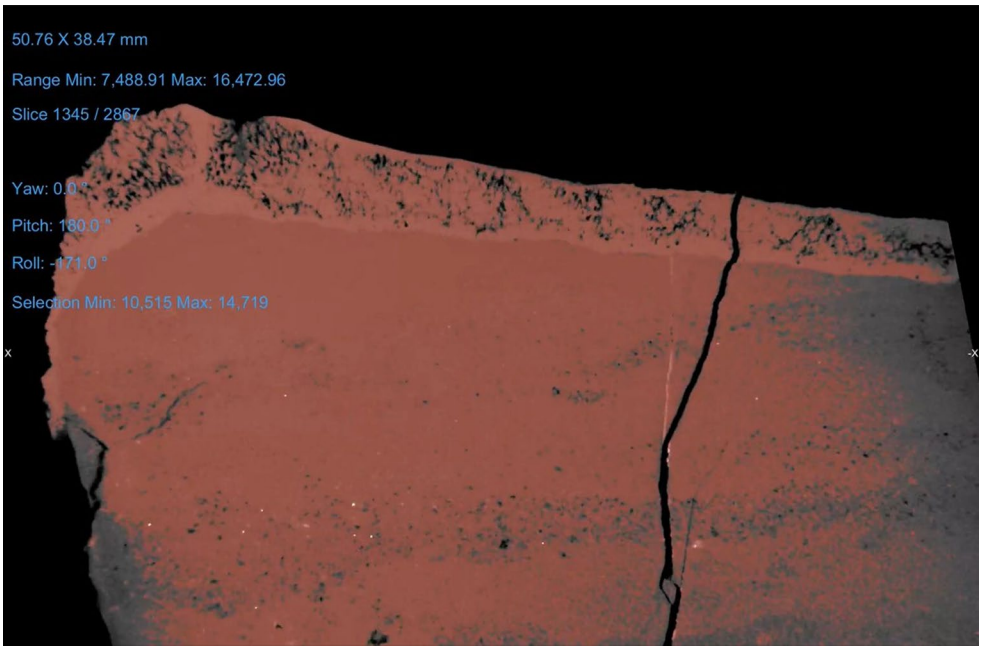

Fig. 8 Video. Video depicting sequential 3D microCT images of longitudinal and transverse cross-sections of the *Palaeopascichnus* specimen from the Upper Member of Fara Formation.

process could result from the low-temperature aqueous dissolution of the carbonate-bearing cement in the host-lithology along the bedding plane, and subsequent secondary calcite nucleation and growth in different successive steps. The occurrence of a thin layer of calcite precipitate on S_0 further supports such a possibility.

The mineralogical features here described make it impossible to confirm or dismiss any intra/epi-benthic ecological association between this specimen and algal/bacterial mats, as enunciated by the work of Gehling and Droser (2009) and Mángano et al. (2024). On the one hand, the specimen lacks imprints left by overlying mats, and on the other hand, the textural information here presented is inconclusive concerning an underlying bacterial mat substrate, other than speculative possibilities regarding the source of calcium carbonate. Therefore, our data is inconclusive as either a contribution or disproval of the "agronomic revolution" theory. Reports of bacterial/algal mats in the Upper Member of Fara formation are absent from the scientific literature, including the recent study of Callegari et al. (2025).

Taking into consideration the data depicted in Fig. 7d and e, it becomes obvious that the advent of calcite nucleation and oriented growth in chambers, hence, forming drusy aggregates, occurred in a similar pattern across all modules, from the bottom of chambers branching out towards the upper wall. Since there is not any noticeable structural discontinuity interrupting the transitions among chambers, it is likely that the chambered arrangement could have been linked by a channel-like structure. Furthermore, from the current observations it is possible to affirm that *Palaeopascichnus* was not necessarily formed by flattened chambers, since the specimen from the Fara Formation displays modules almost as thick as they are wide (Fig. 7c-e), before nearing the bifurcation.

The increase in width as modules approach the point where a bifurcation occurs is a feature that had been previously observed in other specimens of this organism (e.g. Dong et al. 2008; Antcliffe et al. 2011; Kolesnikov et al. 2018). Figure 7b displays a disturbance in the regular morphology of chambers, affecting the two modules preceding the wide, double-hinged chamber. More specifically, there is an inversion in the polarity of chamber convexity; an added element of complexity similar to the features described by Antcliffe et al. (2011). Alongside the biometric indicator of width variation, the shape of chambers with the convex side facing towards the bifurcated extremity may indicate the growth direction of this organism. In the present case, the overall module shape is quite reminiscent of *Palaeopascichnus jiumenensis* specimens reported by Dong et al. (2008), although exhibiting larger overall dimensions. Fig. 8 displays a video, showing sequences of both transverse and longitudinal cross-sections of the specimen under study.

Not only *Palaeopascichnus jiumenensis* specimens are remarkably smaller than any other described palaeopascichnids elsewhere, but also their chambers´ shape differs from the typical globular or allantoid morphologies that characterize these organisms. We speculate that the specimen from the Fara Formation could correspond to an adult individual of *Palaeopascichnus jiumenensis*, based exclusively on morphological similarities, though its dimensions are closer to *Palaeopascichnus linearis*. Therefore, the possibility of a new species, related to unique morphological characteristics and dimensions, remains open for the specimen from the Fara Formation. The insufficient density contrasts within

the carbonate precipitate (i.e. drusy growths) comprising the fossilized structures is problematic for obtaining well-defined three-dimensional volumetric measurements of the chambers, by means of microCT. Nevertheless, morphological measurements indicate that relative module volume increases towards the direction of the bifurcation, being chamber width the main contributor to volume variation.

Kolesnikov et al. (2018) described the striking morphological similarities between *Palaeopascichnus linearis* and *Aschemonella monile*, a modern xenophyophore, focusing on the shared modular organization and possible paleoecological affinities. Beside chamber structure, the last authors point out that superficial modular perforations, found in modern xenophyophores, seem to be absent in all preserved specimens of *Palaeopascichnus*. Antcliffe et al. (2011) make a similar observation, while listing other morphological and stratigraphical features disqualifying a phylogenetic association between the two organisms. Such discussion is naturally out of the scope of the present investigation, nevertheless the combination of taphonomic and post-taphonomic characteristics associated to the preservation of *Palaeopascichnus* are not ideal to the conservation of minute structures, such as superficial sutures and/or pores. In fact, Xiao et al. (2005) stressed the inadequate morphological resolution associated to most Ediacaran fossils, preserved as casts or moulds in siliciclastic rocks. Furthermore, Kolesnikov and Desiatkin (2022) suggested that *Palaeopascichnus jiumenensis* resembles representatives of the ichnogenus *Nenoxites* (Rogov et al. 2012; Luo and Miao 2020) and therefore should be eliminated from the genus *Palaeopascichnus*. However, such criteria seem to be highly arguable, since in fact the morphology of *P. jiumenensis*, as illustrated by Dong et al. (2008), is remarkably different from *Nenoxites*. The presently discussed specimen, clearly not an ichnofossil, also does not fit in the classification of species for *Palaeopascichnus* genus proposed by Kolesnikov and Desiatkin (2022), due to a lack of morphological correspondence. Finally, the specimen from Oman occurs in a quartz siltstone, reflecting an optimal sedimentary environment for *Palaeopascichnus delicatus* and *gracilis*, and near optimal to *P. linearis*, according to the last authors. The wide distribution frequency of species among different sedimentary environments, as evidenced by Kolesnikov and Desiatkin (2022), is a testament to the palaeoecological success of Palaeopascichnids.

The excellent preservation of the specimen from Oman becomes patent through the combination of analytical techniques with different spatial resolution, leading to the first three-dimensional reconstruction of *Palaeopascichnus* in the scientific literature. Other 3D reconstructions of fossils have provided crucial data to sort out biostratigraphical, ecological and phylogenetic affiliation issues (e.g. Meyer et al. 2014; Muto et al. 2021), while X-ray microtomographic techniques have also been employed to probe the functional profile of biomineralized structures (e.g. Neues and Epple 2018; Checa et al. 2020). We hope, therefore, that the methodology developed in the present study paves the way for future research concerning the three-dimensional characterization of fossilized organisms.

Conclusions

The *Palaeopascichnus* specimen from the Fara Formation (Wadi Bani Awf, Oman), represents a unique taphotype of this Ediacaran organism, as a fully developed positive epirelief formed by drusy calcite crystals growth on a bedding plane. The high degree of preservation of this specimen allows a more accurate view of the inner morphology of chambers, given the well-developed module thickness, absent in other occurrences. Microtomographic data concerning both chamber dimensions and morphology does not confirm an accurate affiliation with any currently known species of *Palaeopascichnus*, despite the striking morphological resemblances to *P. jiumenensis*, which yields much smaller specimens. Therefore, the possibility that this specimen represents a new species remains open.

Supplementary Information The online version contains supplementary material available at https://doi.org/10.1007/s10347-025-00705-5.

Acknowledgements This investigation was funded under the Ministry of Science and Innovation (Spain) grant PID2020116660GB-I00 (MCIU/AEI/FEDER/UE) and the European Regional Development Fund (ERDF) - Next Generation/EU program. The authors would like to acknowledge the technical support provided by the staff of the Scientific Instrumentation Center of the University of Granada. An additional acknowledgement is due to Dr. Matthias López Correa for his detailed revisions and sound suggestions, which have greatly improved the scientific quality of the present article.

Author contributions AJP was responsible for petrographic studies, SEM-EDS and microCT data acquisition and interpretation. PAL contributed with XRD measurements and their integration with SEM-EDS data, while also participating in microCT analytical tasks. IC and AS were both responsible for all fieldwork and compiling the necessary information regarding regional geology.

Funding Open Access funding provided thanks to the CRUE-CSIC agreement with Springer Nature.

Data Availability The fossil specimen is property of the Sultanate of Oman, where it will be incorporated at a curated collection at the National History Museum of Oman, with appropriate traceable labeling and documentation, once research has been concluded. Micro-CT data is too large to be hosted in a public repository but is also available for consultation upon request. The remainder of the data generated or analyzed during this study is included in this published article.

Declarations

Competing interests The authors do not have any conflict of competing interests to declare.

References

Acenolaza GF, Germs GJB, Acenolaza FG (2009) Trace Fossils and the Agronomic Revolution at the Neoproterozoic-Cambrian Transition in Southwest Gondwana. In: Gaucher C., Sial, AN, Halverson, GP, Frimmel, HE (eds) Neoproterozoic-Cambrian Tectonics, Global Change and Evolution: a focus on southwestern Gondwana. Developments in Precambrian Geology 16, Elsevier, pp 339–347

Amthor JE, Grotzinger JP, Schröder S, Bowring SA, Ramezani J, Martin MW, Matter A (2003) Extinction of Clodina and Namacalathus at the Precambrian-Cambrian boundary in Oman. Geology 31: 431–434. https://ui.adsabs.harvard.edu/link_gateway/2003Geo… A/https://doi.org/10.1130/0091-7613(2003)031%3C0431:EOCANA%3E2.0.CO;2

Antcliffe JB, Gooday AJ, Brasier MD (2011) Testing the protozoan hypothesis for Ediacaran fossils: a developmental analysis of *Palaeopascichnus*. Palaeontology 54(5):1157–1175. https://doi.org/10.1111/j.1475-4983.2011.01058.x

Béchennec F, Roger J, Le Métour J, Wyn R (1992) Geological map of seeb, sheet NF 40–03, scale 1:250,000, with explanatory notes. Directorate General of Minerals, Oman Ministry of Petroleum and Minerals

Beurrier M, Béchennec F, Rabu D, Hutin G (1986) Geological map of rustaq, sheet NF 40-03D, scale 1:100,000, with explanatory notes: directorate general of minerals. Oman Ministry of Petroleum and Minerals

Bowring SA, Grotzinger JP, Condon D, Ramezani J, Newall M, Allen PA (2007) Geochronology constraints on the chronostratigraphy framework of the neoproterozoic Huqf supergroup, Sultanate of Oman. Am J Sci 307:1097–1145. https://doi.org/10.2475/10.2007.01

Brasier M, McCarron G, Tucker R, Leather J, Allen P, Shields G (2000) New U-Pb Zircon dates for the neoproterozoic Ghubrah glaciation and for the top of the Huqf supergroup, Oman. Geology 28:175–178. https://doi.org/10.1130/0091-7613(2000)28%3C175:NUZDFT%3E2.0.CO;2

Callegari I, Scharf A, Mattern F, Bauer W, Pinto AJ, Rarivoarison H, Scharf K, Al Kindi M (2020) Gondwana accretion tectonics and implications for the geodynamic evolution of Eastern arabia: first structural evidence of the existence of the Cadomian orogen in Oman (Jabal Akhdar dome, central Oman Mountains). J Asian Earth Sci 187:104070. https://doi.org/10.1016/j.jseaes.2019.104070

Callegari I, Scharf A, Pinto AF, Mattern F, Mazumder R, Datta D, Rarivoarison H (2025) Tectonostratigraphy of the Ediacaran Fara formation of the central Oman mountains (Jabal akhdar, Sultanate of Oman): implications for the Late Neoproterozoic evolution of the Eastern Arabian Plate. Precambrian Res 426:107825. https://doi.org/10.1016/j.precamres.2025.107825

Checa AG, Linares F, Maldonado-Valderrama J, Harper EM (2020) Foamy oysters: vesicular microstructure production in the *Gryphaeidae* via emulsification. J R Soc Interface 17(170):20200505. https://doi.org/10.1098/rsif.2020.0505

Cohen KM, Finney SC, Gibbard PL, Fan J-X (2013) The ICS international chronostratigraphic chart. Episodes 36:199–204. https://doi.org/10.18814/epiiugs/2013/v36i3/002

Cope JCW (1982) Precambrian fossils of the Carmarthen area, dyfed. Nat Wales (New Series) 1(2):11–16

Cozzi A, Grotzinger JP, Allen PM (2004) Evolution of a terminal neoproterozoic carbonate ramp system (Buah formation, Sultanate of Oman): Effects of basement paleotopgraphy. Geol Soc Am Bull 116(11–12):1367–1384. https://doi.org/10.1130/B25387.1

Dong L, Xiao S, Shen N, Zhou C (2008) Silicified horodyskia and *Palaeopascichnus* from upper Ediacaran Cherts in South china: tentative phylogenetic interpretation and implications for evolutionary statis. J Geol Soc Lond 165:367–378. https://doi.org/10.1144/0016-76492007-074

El-Ghali MAK, Hersi OS, Abbasi I, Al-Awah H, Moustafa MSH (2021) U-Pb age dating for carbonate sequences: an example from late neoproterozoic Kharus formation, al Jabal al-Akhdar, Northern Oman. In: Çiner A, Banaerjee S, Lucci F (eds) Recent research on sedimentology, stratigraphy, paleontology, tectonics, geochemistry, volcanology and petroleum geology. Springer, Istanbul, pp 79–82. https://doi.org/10.1007/978-3-031-43222-4_17

Fedonkin MA (1981) White Sea Biota of Vendian: Precambrian Non-Skeletal Fauna in the Russian Platform North. In: Keller BM (ed) Transactions of the Geological Institute 342, Nauka (in Russian), Moscow, pp 1-100

Forbes GA, Jansen HSM, Schreurs J (2010) Lexicon of Oman subsurface stratigraphy. Reference guide to the stratigraphy.of oman's hydrocarbon basins, vol 5. Gulf Petrolink, Bahrain

Gehling JH, Droser ML (2009) Textured organic surfaces associated with the Ediacara biota in South Australia. Earth-Sci Rev 96:196–206. https://doi.org/10.1016/j.earscirev.2009.03.002

Glaessner MF (1985) Trace fossils from the precambrian and basal cambrian. Lethaia 2:369–393. https://doi.org/10.1111/j.1502-3931.1969.tb01258.x

Glennie KW, Boeuf MGA, Hughes Clarke MW, Moody-Stuart M, Pilaar W, Reinhardt BM (1974) Geology of the Oman mountains. Kominklijk Nederlands Geologisch En Mijnbouwkundig Genootdschap Trans 31(1):423

Haines PW (2000) Problematic fossils in the late neoproterozoic Wonoka formation, South Australia. Precambrian Res 100:97–108. https://doi.org/10.1016/S0301-9268(99)00070-4

Hawco JB, Kenchington CG, McIlroy D (2019) A quantitative and statistical discrimination of morphotaxa within the Ediacaran genus *Palaeopascichnus*. Pap Palaeontol 7(2):1–17. https://doi.org/10.1002/spp2.1290

Jensen S, Högström A, Høyberget M, Meinhold G, McIlroy D, Ebbestad JOR, Taylor WL, Agic H, Palacios T (2018) New occurrences of *Palaeopascichnus* from the stáhpogieddi formation, Arctic norway, and their bearing on the age of the Varanger ice age. Can J Earth Sci 55(11):1–9. https://doi.org/10.1139/cjes-2018-0035

Kolesnikov A, Desiatkin V (2022) Taxonomy and palaeoenvironmental distribution of palaeopascichnids. Geol Mag 159:1175–1191. https://doi.org/10.1017/S0016756822000437

Kolesnikov A, Rogov VI, Bykova NV, Danilian T, Clausen S, Maslov AV, Grazhdankin DV (2018) The oldest skeletal macroscopic

organism *Palaeopascichnus linearis*. Precambrian Res 316:24–37. https://doi.org/10.1016/j.precamres.2018.07.017

Kolesnikov AV, Latysheva IV, Shatsillo AV, Kusnetsov AB, Kolesnikov AS, Desiatkin VD, Romanyuk TV (2023) Ediacara-type biota in the upper cambrian of the Timan range (Dhzezhim–Parma hill, Komi Republic). Dokl Earth Sci 510(1):289–292. https://doi.org/10.31857/S2686739722602964

Luo C, Miao L (2020) A Horodyskia-Nenoxites-dominated fossil assemblage from the Ediacaran-Cambrian transition (Liuchapo formation, Hunan Province): its paleontological implications and stratigraphic potential. Palaegeograf Palaeocl 545:109635. https://doi.org/10.1016/j.palaeo.2020.109635

Mángano MG, Buatois LA, Minter NJ, Gougeon R (2024) Bioturbators as ecosystem engineers in space and time. Palaeontology 67(6):e12732. https://doi.org/10.1111/pala.12732

Mattern F, Scharf A (2019) Transition from the Hajir formation to the Muaydin formation: a facies change coinciding with extensional, syndepositional faulting (Ediacaran, Jabal akhdar, central Oman Mountains). J Afr Earth Sci 152:237–244. https://doi.org/10.1016/j.jafrearsci.2019.02.016

Mattes BW, Conway Morris S (1990) Carbonate/evaporate deposition in the late Precambrian– Early cambrian Ara formation of Southern Oman. Geol Soc Sp 49:617–636. https://doi.org/10.1144/GSL.SP.1992.049.01.37

McIlroy D, Brasier MD (2017) Ichnological evidence for the cambrian explosion in the Ediacaran to cambrian succession of tanafjord, finnmark, Northern Norway. In: Brasier AT, McIlroy D, McLoughlin N (eds) Earth system evolution and early life: a celebration of the work of Martin brasier. Geological Society Special, London, pp 351–368. https://doi.org/10.1144/SP448.7

Meyer M, Elliot D, Wood AD, Polys NF, Colbert M, Maisano JA, Vickers-Rich P, Hall M, Hoffman KH, Schneider G, Xiao S (2014) Three-dimensional micro-CT analysis of the Ediacara fossil *Pteridiniun simplex* sheds new light on its ecology and phylogenetic affinity. Precambrian Res 249:79–87. https://doi.org/10.1016/j.precamres.2014.04.013

Muto S, Shinsuke Y, Takahashi S, Murayama M (2021) Identification of conodont fossils in pelagic deep-sea silicious sedimentary rocks using laboratory-based X-ray computed microtomography. Lethaia 54(5):687–699. https://doi.org/10.1111/let.12432

Neues F, Epple M (2018) X-ray microcomputer tomography for the study of biomineralized endo- and exoskeletons of animals. Chem Rev 108(11):4734–4741. https://doi.org/10.1021/cr078250m

Palij VM (1976) Remains of soft-bodied animals and trace fossils from the upper precambrian and lower cambrian of Podolia. In: Palij VM, Ryabenko VA (eds) Palaeontology and stratigraphy of the upper precambrian and lower paleozoic of the Southwest part of the East-European platform. Naukova Dumka (in Russian), Kiev, pp 637–677

Palij VM, Posti E, Fedonkin MA (1979) Soft-bodied metazoa and trace fossils of vendian and lower cambrian. Upper precambrian and cambrian.Paleontology of East-European platform. Nauka, Kiev, pp 49–82

Pinto AJ, Sánchez-Pastor N, Callegari I, Pracejus B, Scharf A (2020) Challenges to rutile-based geoscientific tools: low-temperature polymorphic TiO_2 transformations and corresponding reactive pathways. Sci Rep-UK 10:7445. https://doi.org/10.1038/s41598-020-64392-8

Rogov VI, Marusin V, Bykova N, Goy Y, Nagovitsin K, Kochnev B, Karlova G, Grazhdankin D (2012) The oldest evidence of bioturbation on Earth. Geology 40:395–398. https://doi.org/10.1130/G32807.1

Scharf A, Callegari I, Mattern F, Scharf K, Carminati E (2021a) Triple folded surface morphology of neoproterozoic rocks (Jabal Akhdar dome, Oman Mountains) - insights into buttressing effects and regional tectonics. J Asian Earth Sci 221:104942. https://doi.org/10.1016/j.jseaes.2021.104942

Scharf A, Mattern F, Al-Wardi M, Frijia G, Moraetis D, Pracejus B, Bauer W, Callegari I (2021b) The geology and tectonics of the Jabal Akhdar and Saih Hatat domes, Oman mountains, vol 54. Geol Soc London, Memoirs, p 124. 1https://doi.org/10.1144/M54

Seilacher A (2007) Trace fossil analysis. Springer-, Berlin, Heidelberg, New York, p 226

Seilacher A, Mrinjek E (2011) Benkovac stone (Eocene, Croatia): a deep-sea Plattenkalk? Swiss J Geosci 104(1):159–166. https://doi.org/10.1007/s00015-011-0051-7

Seilacher A, Grazhdankin D, Legouta A (2003) Ediacaran biota: the dawn of animal life on the shadow of giant protists. Paleontol Res 7:43–54. https://doi.org/10.2517/prpsj.7.43

Seilacher A, Buatois L, Mángano MG (2005) Trace fossils in the Ediacaran-Cambrian transition: behavioral diversification, ecological turnover and environmental shift. Palaeogeograf Palaeocl 227:323–356. https://doi.org/10.1016/j.palaeo.2005.06.003

Xiao S, Shen B, Chuanming Z, Guwei X, Yuan X (2005) A uniquely preserved Ediacaran fossil with direct evidence for a quilted bodyplan. P Natl Acad Sci USA 102(29):10227–10232. https://doi.org/10.1073/pnas.0502176102

Yuan X, Chen Z, Xiao S, Zhou C, Hua H (2011) An early Ediacaran assemblage of macroscopic and morphological differentiated eukaryotes. Nature 470:390–393. https://doi.org/10.1038/nature09810